Available online at www.sciencedirect.com
ScienceDirect
Applied Surface Science 253 (2007) 3455–3463
applied surface science
www.elsevier.com/locate/apsusc

Morphological, microstructural and optical properties supremacy of binary composite films—A study based on Gd_2O_3/SiO_2 system

N.K. Sahoo *, S. Thakur, R.B. Tokas, A. Biswas, N.M. Kamble

Spectroscopy Division, Bhabha Atomic Research Centre, Trombay, Mumbai 400 085, India

Received 17 February 2006; received in revised form 13 July 2006; accepted 13 July 2006
Available online 22 August 2006

Abstract

Composites are pragmatic choices for tailoring the material to have a desired property. Besides, such thin films have scopes to display superior optical, microstructural and morphological properties which are otherwise not possible to obtain from the pure component films. Vapor-phase-mixed binary composite Gd_2O_3/SiO_2 thin film is one such interesting system where band gap as well as refractive index superiority is observed simultaneously under certain compositional mixings. Such and similar observations in composites cannot be explained by Moss empirical rule. Our systematic study on the microstructure of this composite system based on ellipsometry and scanning probe microscopy has satisfactorily provided the information that can explain such optical properties supremacy. Morphological measurements and its derived parameters like autocorrelation and height–height correlation functions have provided several clues that represent the superior grain structures of the composites. Besides, refractive index modeling through effective single oscillator model has strongly supported such analysis results favoring the superior microstructure in composite films.

PACS: 42.79.Wc; 78.66.−w; 78.20.Ci; 61.16.Ch; 51.70.+f; 52.70.Kz

Keywords: Optical coatings; Optical thin films; Co-deposition; Electron beam evaporation; Ellipsometry; Atomic force microscopy; Composite films; Correlation functions

1. Introduction

The need for advanced materials endowed with enhanced properties has progressively focused on composite systems which can involve complex stoichiometries and/or microstructures [1–3]. Composite films have extended boundaries of possible applications in the field of thin film material sciences [4,5]. For example, many unusual optical coating requirements can be readily addressed by the evolving technology of gradient-index tunable optical thin films [6]. When it comes to such composite microstructure, a host of superior characteristics begin to appear that overcome the limits of the individual component materials [7,8]. The properties which are beyond comprehension can be easily achieved through mixing of materials both in vapor phase and solid solution based techniques. One such application is the development of optical coating materials for deep or extreme ultraviolet (DUV/EUV) region of the electromagnetic spectrum, which has been a very demanding zone with respect to several frontier technological applications related to photonics and spectroscopy [9]. The most important portion of it which represents state-of-the-art in both lasers and optical coatings are the deep ultraviolet (DUV) wavelengths below 0.25 μm. Technologically, DUV-laser coatings and materials have applications in laser ablation, laser spectroscopy, fluorescence stimulation in bio-medical applications and more recently, in semiconductor photolithography of ever-decreasing dimensions in microprocessor manufacturing. Most of the optical coating materials, which are transparent in the visible region, become highly absorbing in the UV region. Thus, this spectral region has been posing considerable challenges with respect to appropriate materials and their combinations especially high refractive index refractory oxide thin film materials [10]. However, binary composite thin films have shown their potentiality as well as possibility to come up to the expectation in satisfying the requirements in this spectral region [11]. There are two primary

* Corresponding author. Tel.: +91 22 25593871; fax: +91 22 25505151.
E-mail address: nksahoo@apsara.barc.ernet.in (N.K. Sahoo).

0169-4332/$ – see front matter © 2006 Elsevier B.V. All rights reserved.
doi:10.1016/j.apsusc.2006.07.048

aspects in the physical significances of such composite films. One of those is the tunability or tailoring of material properties and the other being the superior microstructure [12,13]. In this work such a composite thin film binary system of Gd_2O_3/SiO_2 has been presented which depicted both the morphological densifications and refractive index supremacy over the pure dielectric component films under specific compositional mixings under lower silica fractions. Such favorable properties can be utilized in extending the range of tailoring of the refractive index for the optical multilayer device development programs. Most interestingly, this superior quality is beyond the explanation of Moss empirical rule as discussed in the following section [14,15].

2. Composite films and microstructural supremacy

Mixing material in vapor phase can lead to certain microstructural evolution which sometimes cannot be modeled or explained through the techniques used for conventional optical materials and thin films. One such example is the popular inverse or reciprocal rule that relates the refractive index (n) to the band or energy gap (E_g) in most oxide dielectrics and semiconductor materials. This law which is known as ''Moss rule'' establishes an inverse relationship between the material refractive index with its energy gap, i.e., for dielectrics and semiconductors the higher the refractive index the lower is the band gap. This semi-empirical relationship is based on the fundamental principle that in a dielectric medium all energy levels are scaled down by a factor of square of the dielectric constant (ε^2) or fourth power of the refractive index (n^4). Mathematically it is given by [14–20],

$$E_g n_s^4 = \text{Const.} \quad (1)$$

where E_g is the band or energy gap and n_s is the high frequency refractive index of the dielectric or semiconductor. Such a relation initially was proposed for the photoconductors with constant = 95 eV and later extended to several other semiconductors and dielectrics with somewhat different values for the energy constant parameter. This rule distinctly signifies the reason behind the scarcity of low loss (optical) high index dielectric materials in the lower wavelengths like deep ultraviolet region of the electromagnetic spectrum. However, there are some cases involving composite semiconductors that have violated this reciprocal law [21,22]. It is also interesting to note that violation of Moss rule has always been manifested in achievement of very unusual type of favorable microstructural properties from the dielectric or semiconductor systems. For example, in gain-guided semiconductor lasers in the junction plane and also in the plane perpendicular to the junction, a reduction in band gap involves a refractive-index decrease (e.g., active InAs on GaSb substrate) [23]. The present gadolinia–silica composite films also belong to a similar category and it has opened up an interesting dimension to the applications by displaying both refractive index and band gap supremacy simultaneously under certain compositional mixing ratios. It means that in case of a vapor-phase mixed composite thin film the range of tunability in refractive index need not to be confined between the low and high index material properties only. The maximum tuning limit can go beyond the value of the high index material. This phenomenon has touched upon a dimension of the microstructure where the morphology and grain structure densifications have dominated in the dielectric polarizability than the stoichiometry. In the past similar cases of superior qualities have been reported in certain other composite systems without any concrete and definite explanation. Mostly researchers hinted towards the possible better density factors (microstructural densifications) or grain structure orderings in such composite systems in displaying these unusual superior properties [24–26]. For example while probing yttria–silica (Y_2O_3/SiO_2) composite system by Feldman et al.; they have very interestingly noticed the increase in the refractive index of some of the composite films with respect to the pure Y_2O_3 films [24]. With the analyses of volume fractions they have inferred a possible densification of the microstructure leading to such an unusual increase. A similar observation on CeO_2–SiO_2 system has been reported by Koo et al. [25]. They have noticed a distinct increase in the refractive index of the composite films when the silica composition is between 20 and 35%. Feldman et al. also have reported refractive index enhancement in zirconia–silica system attributing it to a more probable densification process [26]. In the present work gadolinia–silica system has depicted similar trend in the composition dependent refractive index evolution. We have probed such an interesting microstructural evolution with the help of phase modulated ellipsometry, scanning probe microscopy and its derived correlation functional analyses. Such detailed investigations distinctly demonstrate a grain structure transition leading to a microstructural densification. Composite films with the silica composition 10–20% range have displayed a self-affine type surface morphology with more like an amorphous type of grain structure which implies a definite microstructural densification. The pure gadolinia films, on the other hand, displayed a microstructure dominated with aggregates, mounds or superstructures (localized grain clustering). This aspect was distinctly visible not only in the morphology but also got reflected in the height–height and autocorrelation functions [27,28].

3. Interdependence of macroscopic parameters and microstructure

Most of the explanations presented so far are based on the fact that in thin films there is a strong interdependence between the macroscopic parameters and the microstructure [29–31]. Also in such films, the intrinsic dielectric response of an individual homogeneous region or grain depends on its composition and (if the grain is large enough) on the presence or absence of long-range order or correlation factors. Such order or disorder factors are best described by autocorrelation or height–height correlation functions. Screening charge that develops at the boundaries between grains can cause differences between the local field and the macroscopic applied field. Since the effectiveness of screening depends on the shape and relative size of a grain, its contribution to the

macroscopic dielectric response will also depend on these parameters. The definition of the dielectric function as the dipole moment per unit volume suggests that the magnitude of the dielectric response of a polycrystalline or amorphous film with respect to a standard spectrum can provide a simple, convenient and contactless means of measuring the density of the film. The macroscopic dielectric response of a thin film is therefore connected in an intimate way with the, grain structures, compositional and microstructural parameters that determine its other physical properties. It is probably for these reasons earlier researchers have predicted the microstructural densifications in the composite film through refractive index analyses [24–26]. There are also several other model based techniques such as Tauc–Lorentz (TL) parametric and Wemple and Di Domenico's single-effective oscillator models that can be used to probe the microstructural interaction process deeper [32–34].

With the advent of atomic force microscopy the visualization of microstructure and its derived functional correlation parameters in thin films have added better understanding as well as interpreting physical properties and phenomena. Morphological measurements and other derived factors like autocorrelation and height–height correlation functions have contributed substantially to this understanding. In the present work we have made use of these parametric analyses to explain the superior properties of the certain composite films.

4. Analyses with autocorrelation and height–height correlation functions

Although, at the first sight, thin film morphology appears to be random, a close analysis reveals volumes of correlated properties. The best way the thin film morphology can be probed is by analyzing its autocorrelation function (ACF) as well as height–height correlation function (HHCF) [35]. Spatial autocorrelation is, conceptually as well as empirically, the two-dimensional equivalent of redundancy. It measures the extent, to which the occurrence of an event in a designated unit constrains, or makes more probable, the occurrence of an event in its neighboring unit. In other words, the autocorrelation function can be used to detect non-randomness in surface data as well as to identify an appropriate space or time series model if the data are not random. Within the AFM measurements we usually evaluate the one-dimensional autocorrelation function ($\boldsymbol{A}_x$) determined only from the height profiles ($z_{n+m,1}$ and $z_{n,1}$) in the fast scanning axis which can be evaluated from the discrete ($N \times M$) AFM data values as [36],

$$\boldsymbol{A}_x(\tau_x) = \frac{1}{N(M-m)} \sum_{l=1}^{N} \sum_{n=1}^{M-m} z_{n+m,l} z_{n,l} \tag{2}$$

Here τ_x is the distance between the two points in the x-direction (fast scanning axis) in pixel units and m refers to the current data point. In the present studies several co-deposited thin films of gadolinia–silica systems have been analyzed for their morphologies as well as autocorrelation functions using the data and information acquired through the Solver P47H atomic force microscope (AFM) measurements. The autocorrelation functions of pure film and the composites have shown very different trends in their evolution. However, in most of the co-deposited films, such functions can be fitted well with the appropriate realistic Gaussian models. Height–height correlation function is also very intimately associated with the autocorrelation and very prominently represents the grain structures in thin film morphology. Mathematically, it is given by [37],

$$H_x(r_x) = \frac{1}{N(M-m)} \sum_{l=1}^{N} \sum_{n=1}^{M-m} (z_{n+m,l} - z_{n,l})^2 \tag{3}$$

Here H_x is the one-dimensional function and r_x is the distance between the two points in the x-direction (fast scanning axis) in pixel units. In order to get insight into the dynamic behavior and the growth processes related evolution of morphology in the pure and composite films, we calculated the height–height correlation function $H(r)$ based on the AFM data. Like most thin film experiments, here also it is expected that for each film, log $H(r)$ should increase linearly with log r for small distance r, depicting a power-law behavior represented by, $H(r) \propto r^{2\alpha}$, and then leading to saturation for large r. At the initial regime of the correlation function there exist variant slopes representing different microstructural evolutions in composite and pure films. With this concept, we have tried to fit the height–height correlation function with the self-affine properties using the relationship [38],

$$H(r) = 2w^2 \left[1 - \exp\left(- \left(\frac{r}{\xi} \right)^{2\alpha} \right) \right] \tag{4}$$

where r is the relative distance between a pair of points on the surface, w the interface width, α the roughness exponent and ξ is the lateral correlation length. All these parameters have very special significances with the respect to the qualitative as well as quantitative behavior of the surface morphology. For instance, α, the roughness exponent, signifies the how "wiggly" the local slope is. It is also an indicative of the "jaggedness" of the topography as well as signifies the relative contribution of high frequency fluctuations to the roughness. Its value is directly correlated with "*Herst*" exponent that define the fractal dimension of the surfaces. On the very short length scale, this parameter α is connected with the fractal dimension as "$D = 3 - \alpha$". It is worth mentioning that the fractal dimension is the measure of contribution of two- and three-dimensional mechanism during the film growth. Two-dimensional mechanism of growth gives the value of fractal dimension close to two- and three-dimensional close to 3. We consider that fractal dimension is one of the most informative parameter of surface geometry. Moreover, most experimental studies have indicated that fractal dimension and thermodynamic growth condition of film are very much interconnected. The lateral correlation length, ξ, describes the largest distance in which the height is still correlated. It is to be further noted that, ξ provides a length scale which distinguishes the short-range and long-range behaviors of the rough surface. The interface width, w, is a measure of the surface height fluctuation, i.e., it signifies the RMS fluctuation about the mean height.

5. Refractive index modeling

It has already been discussed earlier that the macroscopic parameters and microstructures have a strong interdependence. Results of refractive index dispersion below the interband absorption edge correspond to the fundamental electronic excitation spectrum may assist very important discussion on the dielectric constant of the material. Wemple and Di Domenico have analyzed more than 100 widely different solids and liquids using a single-effective oscillator model [34]. Based upon the validity of Kramers–Kronig relationship, equations for dielectric constants ε_r and ε_i were given by them. Equation for the real part takes the form:

$$\varepsilon_r^2(E) = 1 + \frac{F}{E_0^2 - E^2} \tag{5}$$

where the two parameters E_0 and F have straightforward relations to the electric dipole strength and the corresponding transition frequencies of all oscillators. The parameters used in this expression have fundamental as well as physical significances. By a special combination of parameters, Wemple and Di Domenico defined a microstructural variable E_d as [34]:

$$E_d = \frac{F}{E_0} \tag{6}$$

Combination of the above equations and neglecting values of k in the transparent region gives:

$$\varepsilon_r(E) = n^2(E) = 1 + \frac{E_d E_0}{E_0^2 - E^2} \tag{7}$$

Values of the parameters E_0 and E_d were estimated by plotting $(n^2 - 1)^{-1}$ versus E^2 and fitting the relation to a straight line. These two parameters of the model play significant role in explaining the experimental observations. For example, the dispersion energy E_d that measures the average strength of interband optical transitions is associated with the changes in the structural order of the material. Similarly, the effective oscillation energy E_0 can be directly correlated with the optical band gap by an empirical formula. The increase of the dispersion energy value (E_d) is usually associated with evolution of the thin film microstructure to a more ordered phase [39]. The oscillator energy E_0 is independent of the scale of ε_2 and is subsequently an ''average'' energy gap, where as E_d depends on the scale of ε_2, and thus serves as an interband strength parameter.

6. Experimental details

Under the present investigation, we have carried out some systematic experiments and analysis of co-deposited thin films of Gd_2O_3/SiO_2 system using phase modulated ellipsometry, spectrophotometry and multimode scanning probe microscope (SPM) techniques. The samples were deposited in a fully automatic thin film vacuum system ''VERA-902'' by adopting the reactive electron beam deposition technique. The depositions of the films were carried out using two 8 kW VTD electron beam guns with sweep and automatic emission controls. The film materials for SiO_2 and Gd_2O_3 were chosen from Cerac's batch number ''S-1060'' (purity 99.99%) and ''G-1076'' (purity 99.9%), respectively. The substrate temperature was maintained at 70 °C for the deposited films. The total pressure inside the chamber during the deposition process was maintained at 1×10^{-4} mbar through MKS mass flow controllers. The constituents of the gases present during the deposition were analyzed by a residual gas analyzer (RGA) model; Pffeier's Prisma-200. The film thicknesses were monitored both using the Leybold's OMS-2000 optical thickness monitor (OTM) as well as Inficon's XTC/2 QCM (quartz crystal monitors). The individual rates of depositions were very accurately monitored as well as controlled in automatic mode as per the requirements of the co-deposition process. The proportional, integration and differential (PID) parameters of the thickness as process control system were judiciously optimized in order to avoid unwanted rate fluctuations during co-deposition processes. By such appropriate and accurate rate controls, it was possible to obtain Gd_2O_3/SiO_2 co-deposited composite films with the desired compositions in the ranges of 10–90%. The entire deposition process parameters such as substrate temperature, optical thicknesses, rates of deposition, total reacting gas pressure were monitored and controlled by a Siemen's industrial programmable logic controller (PLC) with appropriate GUI based front-end software. The co-deposited film optical thicknesses were decided to remain 6–8 quarter-wave ($\lambda/4$) at a wavelength (λ) of 600 nm, in order to obtain appropriate numbers of interference fringes for spectrophotometric as well as ellipsometric analysis techniques.

For ellipsometric studies, Jobin Yvon's phase modulated spectroscopic ellipsometer model UVISEL has been employed to analyze the growth dependent spectral optical properties. As described above Tauc–Lorentz formulation and effective single oscillator models have been adopted to probe the co-deposited films for their refractive index profiles using a discrete multilayer approach. For AFM characterization, NT–MDT's solver P-47H multimode ambient-based scanning probe system has been utilized. The cantilever used was a Si_3N_4 with typical spring constant of 0.6 N/m and resonant frequency of 75 kHz. We have adopted the contact mode operation without any image filtering technique for the topographic measurements. For Fourier analysis, the built-in FFT module of the control software ''NOVA-SPM'' was employed to generate the mappings. Similarly, for autocorrelation function analysis the built in features are employed to compute both the 2-D and 3-D ACF parameters. In order to have the consistency in the experimental results, the same cantilever was used for all the topographic measurements. All the co-deposited films were spectrally measured for their reflectance as well as transmittance characteristics using Shimadzu UV3101PC spectrophotometer system equipped with an integrating sphere accessory. The results of various characterization techniques have been presented in the subsequent section.

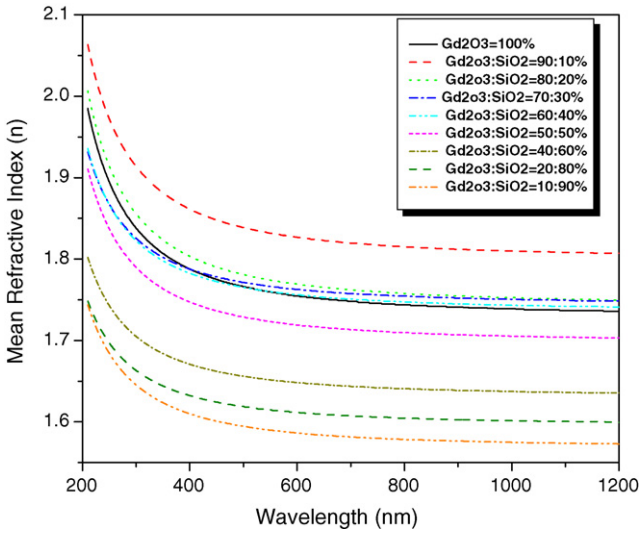

Fig. 1. Tailoring of spectral mean refractive indices of various gadolinia–silica composite thin films prepared with various composition ratios from 90:10 to 10:90.

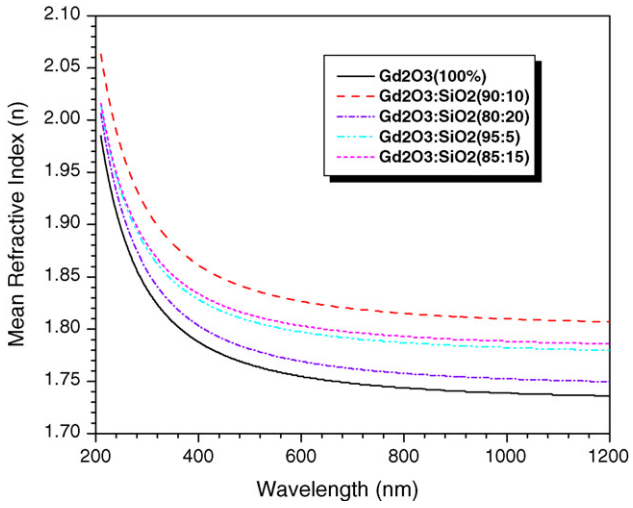

Fig. 2. Depiction of superior spectral refractive indices of gadolinia–silica composite films with 90:5, 90:10, 85:15 and 80:20 compositions over the pure Gd_2O_3 (100%) thin film. In this graph data on lower silica fraction has been zoomed out with respect to the mixing compositions.

7. Results and discussions

In the present experiment, several co-deposited composite films with the Gd_2O_3/SiO_2 compositions in the mixing range from 10:90 to 95:5 have been prepared under certain predefined substrate temperature and oxygen partial pressure conditions decided through previous experiments. In Fig. 1 the spectral mean refractive index profiles of pure Gd_2O_3 as well as co-deposited composite Gd_2O_3/SiO_2 thin films with various compositions have been depicted. These spectral refractive index profiles were derived from the measurement and analysis of Ψ and Δ parameters acquired through phase modulated ellipsometry. The refractive index obtained in case of our pure gadolinia film matches very well with the published data of similar films achieved through physical vapor deposition and sol–gel processes [40–43]. In Fig. 1 it is significantly noticed that the refractive index profiles of certain composite films (in the range of 90/10 to 80/20) have depicted superior values in comparison to the pure Gd_2O_3 or SiO_2 films. Also it can be noticed that the applications related to the range of refractive

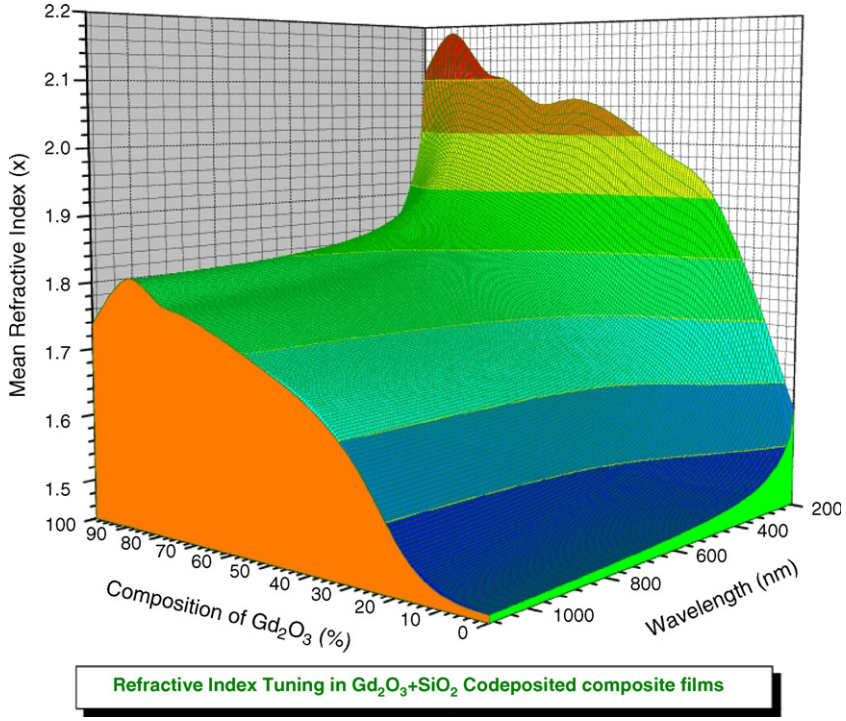

Fig. 3. 3-D plot of spectral refractive index of the gadolinia–silica thin films depicting superior refractive index of certain composite films (in the mixing range of 95/5 to 80/20) over the pure gadolinia (100%) film.

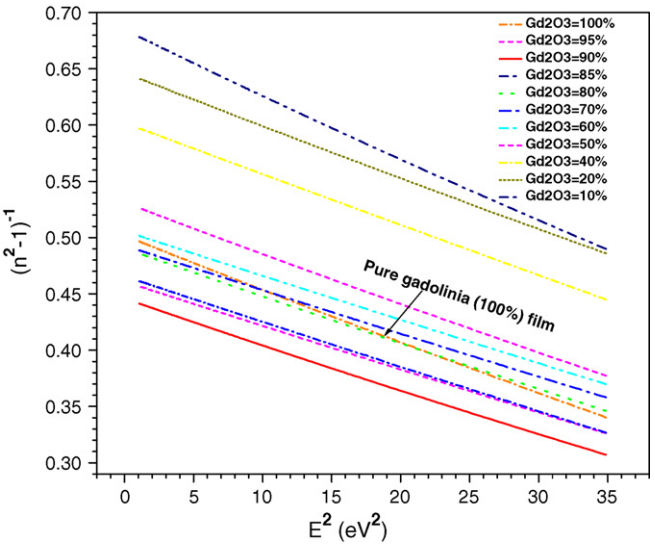

Fig. 4. Plots of $(n^2 - 1)^{-1}$ vs. E^2 of various composite films depicting straight line behavior. The results derived from this plot have been utilized to compute two important parameters E_d and E_0 which represent the dispersion energy and oscillator energy, respectively.

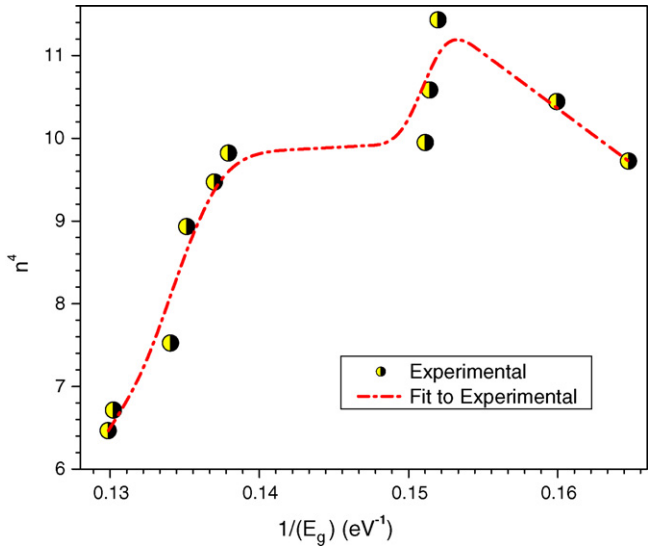

Fig. 6. Plot of n^4 and $1/E_g$ depicting non-linear characteristic and strongly supporting the violation of Moss semi-empirical rule in composite gadolinia–silica films.

index tunability can make use of this extended region very conveniently. Fig. 2 has highlighted this fact where the comparison is made amongst the pure gadolinia and the composite (Gd_2O_3:SiO_2) films with zooming out the experimental co-deposition data under lower silica fractions. From this figure the superior spectral refractive index of the composite film in the silica mixing range of 5–20% can be distinctly noticed. For a more distinct representation we have plotted the 3-D fit to our experimental observation in Fig. 3. It can be seen in this 3-D figure that there is a range of compositions over which the composite films depicted superior spectral refractive index values. In order to analyze the

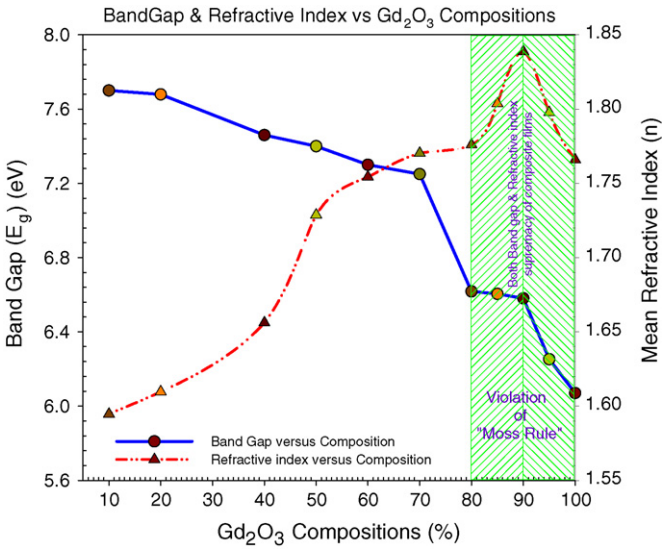

Fig. 5. Variation refractive index (at a wavelength of 600 nm) and band gap in gadolinia–silica composite thin film system. As it can be seen the shaded area depicted a continuous increase in the band gap of the composite film. In this area the numerical values of the refractive index parameter for the composite films are more than the pure gadolinia system.

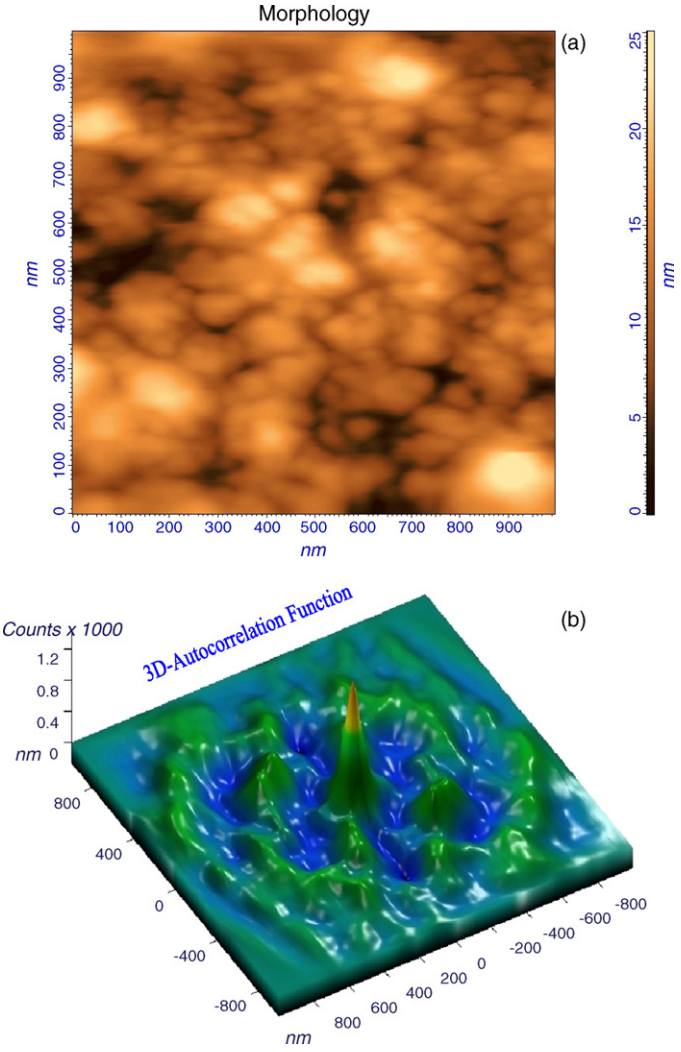

Fig. 7. (a) Morphology and (b) 3-D autocorrelation function of pure gadolinia film depicting the dominance of aggregates or mound structures.

microstructural evolution through effective single oscillator model, we have plotted $(n^2 - 1)$ versus E^2 in Fig. 4. It can be noticed that pure gadolinia film has demonstrated different dispersion behavior in comparison to the most composite films. Also as an added advantage, the composite films are also associated with better band gap values. This result is distinctly depicted in Fig. 5. The shaded region in the plot has highlighted this fact that under these compositions both the refractive index and band gap supremacy can be achieved which is quite different from the monotonic tailoring of the optical properties in conventional composite films. This is a very definite situation of the violation of Moss rule. This violation is highlighted in Fig. 6 where the plot between n^4 and $1/E_g$ has demonstrated an interesting non-linear characteristic. Such situations are highly useful for developing multilayer optical coatings for the deep ultraviolet region utilizing the advantages of the band gap and the refractive index parameters. Such improved optical properties of composite films violating Moss rule have been earlier observed in certain other co-deposited thin film systems [32–34]. Although earlier researchers have only predicted possible microstructural superiority in composite films, we have very authentically verified this observation through atomic force microscopic measurements as well as refractive index modeling. In Fig. 7(a) the topography of the pure gadolinia film has been presented. One can easily see a poor grain structure distribution in the morphology. There are very prominent localized aggregates or mound structures distributed in the morphology. The 3-D-autocorrelation function of this morphology is depicted in Fig. 7(b). The presence of dominating mound structures (grain clustering) is highlighted in this measurement result. Besides, the correlation length has a higher numerical value that supports the presence of such correlated superstructures or aggregates. As a contrast, the composite gadolinia–silica films have shown a denser, amorphous type of grain structures in the morphology presented in Fig. 8(a). The dense morphology looks more like the result that is very much similar to the outcome of ion-assisted deposition. The 3-D-autocorrelation function also supported this observation which can be seen from Fig. 8(b). The autocorrelation function has displayed a more self-affine quality in the analysis result. 2-D analysis depicted in Fig. 9(a and b) of such autocorrelation functions distinctly highlighted such transition of the grain structures from mound to self-affine. Fig. 10 depicted the height–height correlation functional analysis to the morphologies. Such an analysis has also

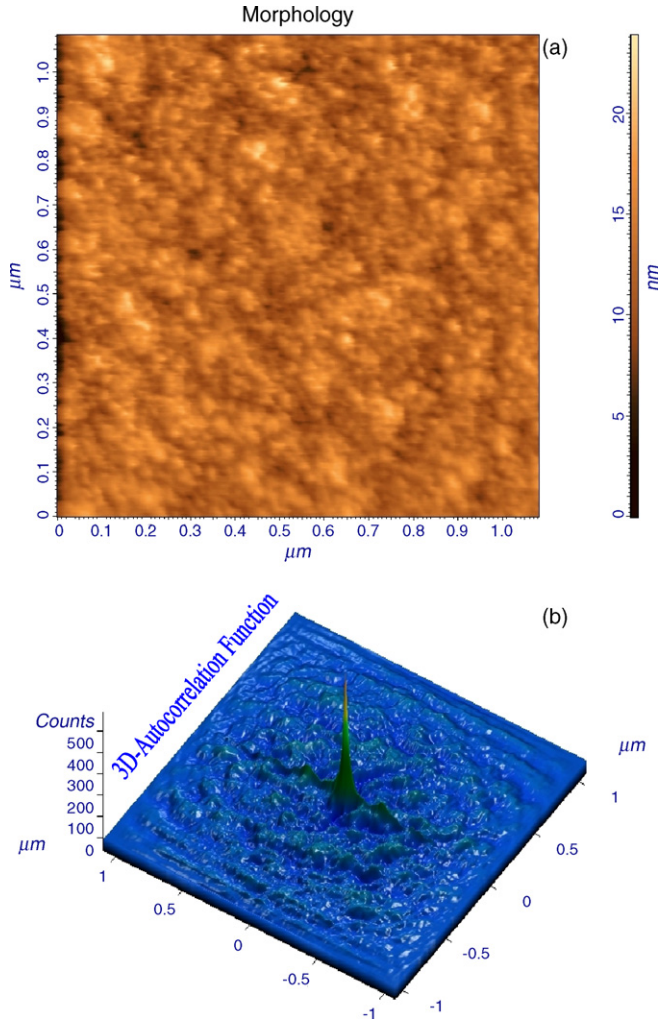

Fig. 8. (a) Morphology and (b) 3-D autocorrelation function of composite gadolinia–silica film depicting a more smooth self-affine micro grain structures.

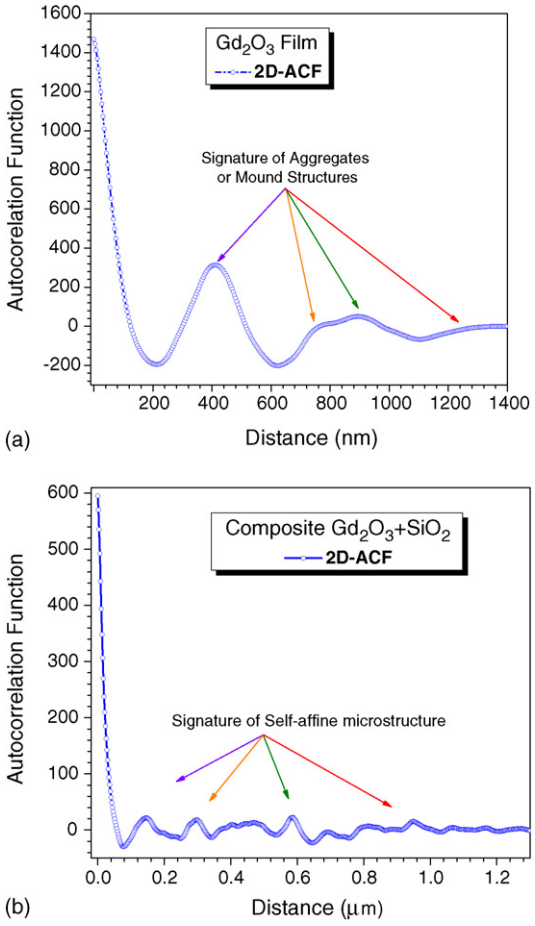

Fig. 9. Two-dimensional autocorrelation function of (a) pure gadolinia (100%) film and (b) composite gadolinia–silica (90/10) film demonstrating mound structure and self-affine nature of the morphology, respectively.

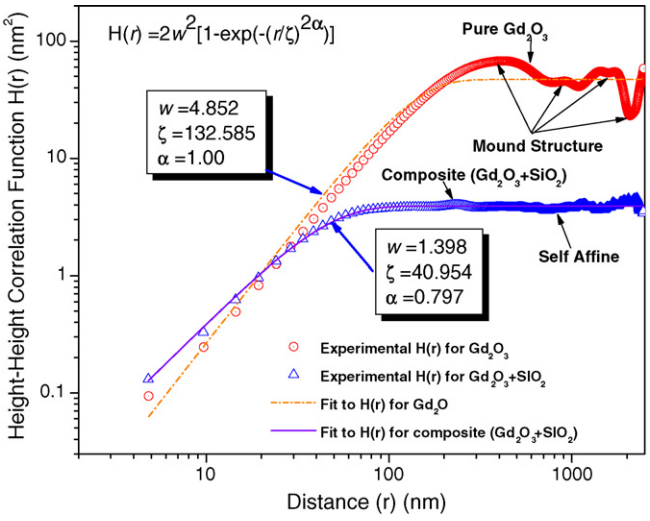

Fig. 10. Two-dimensional height–height correlation of (a) pure gadolinia (100%) and (b) composite gadolinia–silica (90/10) film. The composite film microstructure has a smaller correlation length which represents more like an amorphous and self-affine type of grain structure.

very appropriately highlighted the self-affine nature of the composite film topography. The correlation length for such a structure has depicted a relatively lower value supporting dense and amorphous like quality. Microstructural ordering is also an important parameter which is more or less reflected in the refracting index modeling. Such a result is highlighted through Fig. 11. The structural order parameter E_d of the single oscillator model has shown a very close association with refractive index. This analysis implies that local microstructure ordering can predominantly influence the density and the grain morphology which in turn can lead to a better refractive index value, as is the case with certain composite films with lower silica components.

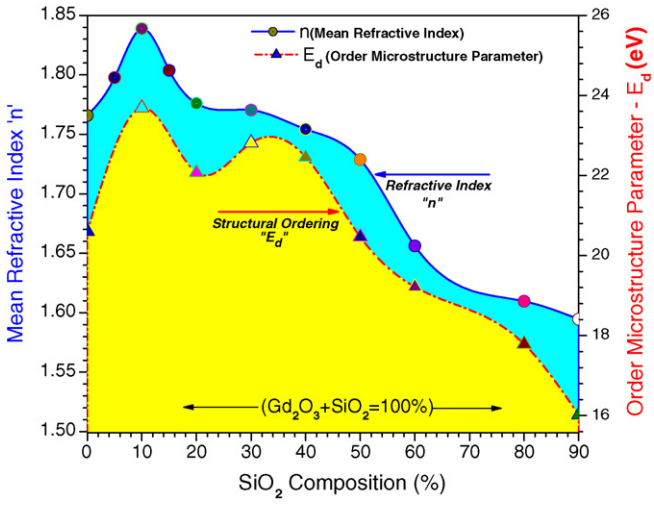

Fig. 11. Analysis of refractive index using the effective single oscillator model. The microstructural ordering parameter, "E_d" can be seen to follow the refractive index evolution. This distinctly points out the structural ordering has a close association with the polarizability that ultimately decides the refractive index property.

8. Conclusion

The refractive index tunability as well as optical and microstructural superiority in gadolinia–silica composite films under certain compositional ratios has been probed with phase modulated ellipsometry and scanning probe microscopy. Spectral refractive index profiles were derived from the ellipsometric parameters through Tauc–Lorentz parameterization. Composite films depicted an evolution in morphology as well as grain structure ordering which are reflected in autocorrelation and height–height correlation functional analysis. The structural ordering parameter of effective single oscillator model followed almost a similar trend as in the evolution of the refractive index. Besides the optical and microstructural properties have shown to violate the most popular "Moss rule" that establishes a reciprocal relation between the refractive index and the energy gap. Although prime objective of such composite structure is to achieve the tunability in the refractive index, as an added advantage some of the composite films depicted superior optical and microstructural properties simultaneously. Such properties can be utilized not only in extending the range of refractive index tunability but also in developing superior multilayer devices in the deep ultraviolet spectral region.

References

[1] L. Armelao, C. Eisenmenger-Sittner, M. Groenewolt, S. Gross, C. Sada, U. Schubert, E. Tondello, A. Zattin, J. Mater. Chem. 15 (2005) 1838.
[2] W.J. Gunning, R.L. Hall, F.J. Woodberry, W.H. Southwell, N.S. Gluck, Appl. Opt. 28 (1989) 2945.
[3] M.F. Ouellette, R.V. Lang, K.L. Yan, R.W. Bertram, R.S. Owles, D. Vincent, J. Vac. Sci. Technol. A 9 (1991) 1188.
[4] J. Chen, S. Chao, J. Kao, H. Niu, C. Chen, Appl. Opt. 35 (1996) 90.
[5] M. Kobayashi, H. Terui, Appl. Opt. 22 (1983) 3121.
[6] R. Jacobsson, Inhomogeneous and coevaporated homogeneous films for optical applications, in: G. Hass, M.H. Francombe, R.W. Hoffman (Eds.), Physics of Thin Films, vol. 8, Academic, New York, 1975, pp. 51–98.
[7] H.O. Sankur, J. DeNatale, W.J. Gunning, Appl. Opt. 30 (1991) 497.
[8] H. Sankur, W. Gunning, J. Appl. Phys. 66 (1989) 807.
[9] F. Cheliebou, A. Boyer, L. Martin, Thin Solid Films 249 (1994) 86.
[10] F. Rainer, W.H. Lowdermilk, D. Milam, C.K. Carniglia, T.T. Hart, T.L. Lichtenstein, Appl. Opt. 24 (1985) 496.
[11] N.K. Sahoo, A.P. Shapiro, Appl. Opt. 37 (1998) 698.
[12] H. Demiryont, Appl. Opt. 24 (1985) 2647.
[13] M. Gajdardziska-Josifovska, R.C. McPhedran, D.J.H. Cockayne, D.R. McKenzie, R.E. Collins, Appl. Opt. 28 (1989) 2736.
[14] N.M. Ravindra, J. Narayan, J. Appl. Phys. 60 (1986) 1139.
[15] T.S. Moss, Proc. Phys. Soc. Lond. Sect. B 63 (1950) 167.
[16] J.S. Seeley, R. Hunneman, A. Whatley, Appl. Opt. 20 (1981) 31.
[17] J.R. Dixon, H.R. Riedl, Phys. Rev. 140 (1965) A1283.
[18] M. Bertolotti, V. Bogdanov, A. Ferrari, A. Jascow, N. Nazorova, A. Pikhtin, L. Schirone, J. Opt. Soc. Am. B 7 (1990) 918.
[19] K.L. Vodopyanov, J. Opt. Soc. Am. B 16 (1999) 1579.
[20] R.A. Soref, Appl. Opt. 31 (1992) 4627.
[21] J. Fesquet, J. Opt. Soc. Am. A 3 (1986) 369.
[22] M. Kano, K. Sugiyama, Electron. Lett. 16 (1980) 146.
[23] J. Fesquet, J. Opt. Soc. Am. A 3 (1986) 369.
[24] A. Feldman, X. Ying, E.N. Farabaugh, Appl. Opt. 28 (1989) 5229.
[25] W.H. Koo, S.M. Jeoung, S.H. Choi, S.J. Jo, H.K. Baik, S.J. Lee, K.M. Song, Thin Solid Films 468 (2004) 28.
[26] A. Feldman, E.N. Farabaugh, W.K. Haller, D.M. Sanders, R.M. Stempniak, J. Vac. Sci. Technol. A 4 (1986) 2969.

[27] A. Iraji Zad, G. Kavei, M. Reza Rahimi Tabar, S.M. Vaez Allaei, J. Phys. Condens. Matter 15 (2003) 1889.
[28] D.C. Law, L. Li, M.J. Begarney, R.F. Hicks, J. Appl. Phys. 88 (2000) 508.
[29] E. Pelletier, F. Flory, Y. Hu, Appl. Opt. 28 (1989) 2918.
[30] M. Cevro, Thin Solid Films 258 (1995) 91.
[31] M. Jerman, Z. Qiao, D. Mergel, Appl. Opt. 44 (2005) 3006.
[32] J. Price, P.Y. Hung, T. Rhoad, B. Foran, A.C. Diebold, Appl. Phys. Lett. 83 (2004) 1701.
[33] H. Lee, I.Y. Kim, S.S. Han, B.S. Bae, M.K. Choi, I.S. Yang, J. Appl. Phys. 90 (2001) 813.
[34] S.H. Wemple, M. DiDomenico Jr., Phys. Rev. B 3 (1971) 1338.
[35] H.N. Yang, A. Chan, G.C. Wang, J. Appl. Phys. 74 (1993) 101.
[36] Y. Chen, W. Huang, Meas. Sci. Technol. 15 (2004) 2005.
[37] Z.J. Liu, N. Jiang, Y.G. Shen, Y.W. Mai, J. Appl. Phys. 92 (2002) 3559.
[38] C.H. Zhang, Z.J. Liu, K.Y. Li, Y.G. Shen, J.B. Luo, J. Appl. Phys. 95 (2004) 1460.
[39] S.H. Wemple, Phys. Rev. B 7 (1973) 3767.
[40] A.A. Dakhel, J. Opt. A Pure Appl. Opt. 3 (2001) 452.
[41] A. García-Murillo, C. Le Luyer, C. Garapon, C. Dujardin, E. Bernstein, C. Pedrini, J. Mugnier, Opt. Mater. 19 (2002) 161–168.
[42] H. Guo, X. Yang, T. Xiao, W. Zhanga, L. Lou, J. Mugnier, Appl. Surf. Sci. 230 (2004) 215.
[43] C. Le Luyer, A. García-Murillo, E. Bernstein, J. Mugnier, J. Raman Spectrosc. 34 (2003) 234.